

# Journal of Materials Chemistry C

Accepted Manuscript



This is an *Accepted Manuscript*, which has been through the Royal Society of Chemistry peer review process and has been accepted for publication.

*Accepted Manuscripts* are published online shortly after acceptance, before technical editing, formatting and proof reading. Using this free service, authors can make their results available to the community, in citable form, before we publish the edited article. We will replace this *Accepted Manuscript* with the edited and formatted *Advance Article* as soon as it is available.

You can find more information about *Accepted Manuscripts* in the [Information for Authors](#).

Please note that technical editing may introduce minor changes to the text and/or graphics, which may alter content. The journal's standard [Terms & Conditions](#) and the [Ethical guidelines](#) still apply. In no event shall the Royal Society of Chemistry be held responsible for any errors or omissions in this *Accepted Manuscript* or any consequences arising from the use of any information it contains.

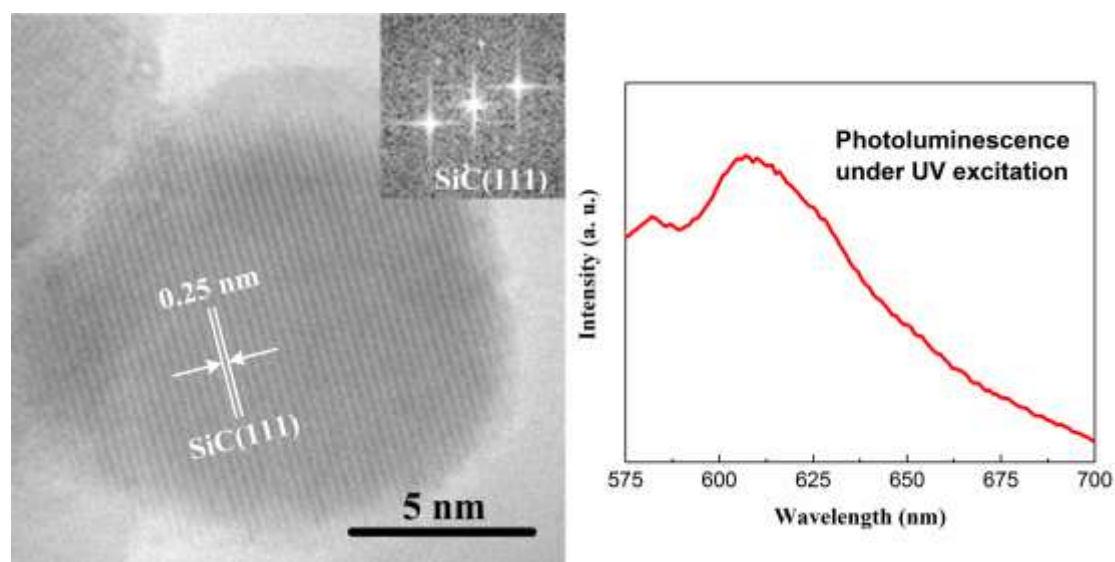
# High rate fabrication of room temperature red photoluminescent SiC nanocrystals

Tengfei Cao, Yan Cheng, Haibao Zhang, Binhang Yan and Yi Cheng\*

Department of Chemical Engineering, Tsinghua University, Beijing, China.

E-mail: yicheng@tsinghua.edu.cn; Fax: +86-10-62772051; Tel: +86-10-62794468

## Table of contents entry



SiC nanocrystals with room temperature red region photoluminescence are fabricated at high rate in atmospheric pressure thermal plasma using  $\text{SiCl}_4$  and  $\text{C}_2\text{H}_2$  as silicon source and carbon source.

## Abstract

High rate fabrication of thin film complex consisting of cubic-SiC nanocrystals, amorphous silicon and graphite was realized by an atmospheric pressure thermal plasma enhanced chemical vapor deposition (APTPECVD) process with  $\text{SiCl}_4$  and  $\text{C}_2\text{H}_2$  as silicon source and carbon source,

respectively. The morphology, crystal structure and surface chemical composition of the products were characterized. The APTPECVD SiC nanocrystals have average diameters between 18-30 nm. A room temperature red region photoluminescence (PL) property originated from quantum confinement effect of these SiC nanocrystals was observed under UV wavelength excitation. Moreover, pure SiC nanocrystals with red region PL property can be obtained after a simple post-treatment including calcining and etching processes. These red photoluminescent SiC nanocrystals could be utilized as biomarkers in bioimaging and drug delivery.

## Introduction

Silicon carbide (SiC) is an important group IV wide band gap semiconductor with superior electronic, thermal and mechanical properties for a large variety of applications, *e.g.* high-power electronics at elevated temperatures, light emitting diodes (LED) and photonic devices.<sup>1-5</sup> However, the indirect band gap of bulk SiC material leads to its weak emission property, which has hampered its application in optical devices.<sup>6</sup> This fact stimulated intensive studies of different polytypes and new forms of SiC.<sup>7, 8</sup> SiC nanocrystals are found to have several excellent properties such as photoluminescence (PL) at room temperature.<sup>9-14</sup> This PL property can be attributed to the formation of a direct band gap and quantum confinement effect in SiC nanocrystals.<sup>15-17</sup> The band gap of SiC nanocrystals is widened as a result of quantum confinement which enhances the PL property and blueshifts the PL peaks.<sup>18-21</sup> With both PL property and biocompatibility, SiC nanocrystals have found their way into biomedical applications, such as *in vivo* bioimaging and drug delivery.<sup>22-27</sup>

Plasma enhanced chemical vapor deposition (PECVD) is a conventional method of fabricating SiC nanocrystals.<sup>28-33</sup> This plasma technique has the ability to dissociate and activate various gas

precursors.<sup>34</sup> Plasma can also sustain gas phase nucleation and the polymerization of nano-sized nucleates in nanomaterial fabrication process.<sup>28</sup> Low pressure cold plasma enhancement is mostly used in the PECVD of SiC nanocrystals even though this method has a relatively low product capability. Thermal plasma has the features of high temperature field, high energy density and high reactive species concentration, which has been applied in the fabrication of nanocrystalline silicon thin films at high deposition rates.<sup>35, 36</sup> SiC nanocrystals covered by carbon films and embedded in the complex of graphite and amorphous silicon (a-Si) have also been fabricated with SiCl<sub>4</sub> and CH<sub>4</sub> as silicon and carbon sources in atmospheric pressure thermal plasma.<sup>37</sup> Moreover, the deposition mechanism has been studied by optical emission spectroscopy (OES).<sup>37, 38</sup> The reason to choose SiCl<sub>4</sub> as the precursor is to utilize the large amount of hazardous by-product SiCl<sub>4</sub> from polysilicon industry. In this work, we aim to produce thin films consisting of SiC nanocrystals by using an atmospheric pressure thermal plasma enhanced chemical vapor deposition (APTPECVD) process with SiCl<sub>4</sub> and C<sub>2</sub>H<sub>2</sub> as silicon and carbon sources, respectively. As the APTPECVD process has the high deposition rate characteristic, it is anticipated that high efficient conversion of SiCl<sub>4</sub> can be achieved, which accordingly would make the mass production of SiC nanocrystals feasible. The high efficient fabrication of SiC nanocrystals has been realized with SiCl<sub>4</sub> and CH<sub>4</sub> as precursors.<sup>37</sup> Efforts are made to study the effect of different carbon sources on deposition process and product properties. In the following contents, the properties of APTPECVD products will be characterized, among which the room temperature red region PL property is to be reported for the first time. Furthermore, a simple post-treatment is carried out to remove graphite and a-Si from the product to receive pure SiC nanocrystals. Considering the high production capability of APTPECVD, this thermal plasma process may be further utilized to fabricate SiC nanocrystals in large scale for

biomedical applications.

## Results and discussion

The crystal structures of the samples were analyzed by X-ray diffraction (XRD) and Raman spectroscopy. Fig. 1 (a) gives the samples' XRD patterns which show the existence of cubic-SiC ( $\beta$ -SiC), a-Si and graphite. Diffraction peaks located at  $35.431^\circ$ ,  $41.278^\circ$  and  $59.869^\circ$  correspond to (111), (200) and (220) crystal planes of  $\beta$ -SiC, respectively. The intensities of diffraction peaks of  $\beta$ -SiC first increase then decrease with increasing  $\text{SiCl}_4$  input rate. The highest diffraction peak intensity is observed at  $\text{SiCl}_4$  input rate of  $0.42 \text{ mol h}^{-1}$ . Diffraction peaks located at  $29.013^\circ$  and  $69.362^\circ$  correspond to (111) and (400) crystal planes of crystalline silicon (c-Si). The broadening of the (111) diffraction peak results from the amorphous feature of silicon in the sample. Besides, diffraction peak of graphite crystal plane (002) at  $25.782^\circ$  is observed in samples with  $\text{SiCl}_4$  input rates of  $0.42$  and  $0.52 \text{ mol h}^{-1}$ . The intensities of  $\beta$ -SiC diffraction peaks are weaker compared with those of samples fabricated with  $\text{SiCl}_4$  and  $\text{CH}_4$  as precursors, which means that samples with  $\text{C}_2\text{H}_2$  as carbon source have fewer amount of SiC.<sup>37</sup> The average grain diameters of SiC nanocrystals calculated according to Scherrer's formula are in the range of 18-30 nm.<sup>39</sup> Raman spectra in Fig. 1 (b) give the same result as XRD patterns. The broad peak at  $\sim 480 \text{ cm}^{-1}$  corresponds to a-Si while peaks at  $\sim 1350$ ,  $\sim 1580$  and  $\sim 2690 \text{ cm}^{-1}$  correspond to graphite's D band, G band and 2D band, respectively.<sup>40, 41</sup> The relatively high intensities of D band and 2D band peaks should originate from the high defect density and nanoscale of graphite in the samples.<sup>42</sup> The a-Si peak becomes higher with increasing  $\text{SiCl}_4$  input rate which signifies the increase of a-Si amount in the sample with increasing  $\text{SiCl}_4$  input rate. The longitudinal optical (LO) phonon peak at  $972 \text{ cm}^{-1}$  and transverse

optical (TO) phonon peak at  $796\text{ cm}^{-1}$  originated from  $\beta\text{-SiC}^{43}$  are not observed during Raman spectroscopy analysis.

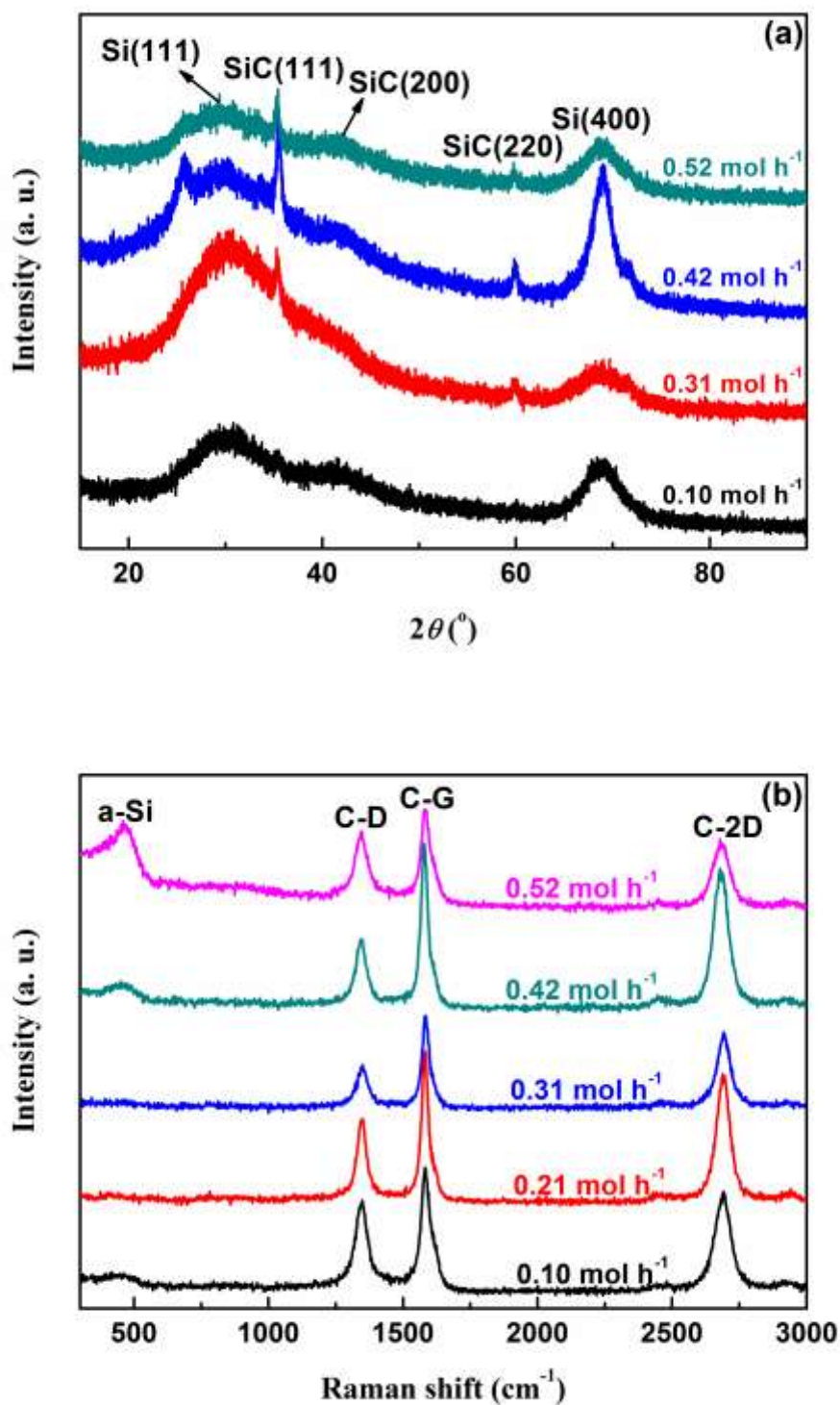


Fig. 1 (a) XRD patterns and (b) Raman spectra of samples deposited at different  $\text{SiCl}_4$  input rates.

The morphology and microstructure of the samples were characterized by scanning electron microscope (SEM) and transmission electron microscope (TEM). Fig. 2 shows the SEM and TEM images of the samples. The sample has a porous coral-like structure. Nano-sized sphere particles are formed on branched skeletons. As can be seen from TEM images, the sphere particles are SiC nanocrystals covered by carbon films, and the skeleton is composed of graphite and a-Si. Since SiC nanocrystals are covered by carbon films, the excitation of these nanocrystals during Raman spectroscopy characterization becomes difficult which explains the absence of  $\beta$ -SiC Raman peaks. Distinguished lattice fringes of (111) crystal plane of  $\beta$ -SiC with interplanar crystal spacing of 0.25 nm and (002) crystal plane of graphite with interplanar crystal spacing of 0.34 nm can be observed, which agrees well with the fast Fourier transformation (FFT) results given in TEM images. These APTPECVD products have similar microstructures with the products of  $\text{CH}_4$  as the carbon source. Nevertheless, less sphere particles are formed with  $\text{C}_2\text{H}_2$  as the carbon source than the case with  $\text{CH}_4$  as the carbon source, which well explains why the diffraction peaks intensities of  $\beta$ -SiC with  $\text{C}_2\text{H}_2$  as the carbon source are lower than those with  $\text{CH}_4$  as the carbon source.<sup>37</sup> The deposition rate of the thin film complex is then calculated based on the film thickness measured by SEM as shown in Fig. 2 (a). The effect of  $\text{SiCl}_4$  input rate on the deposition rate is given in Fig. 3. The deposition rate increases with increasing  $\text{SiCl}_4$  input rate and reaches higher than  $100 \text{ nm s}^{-1}$  after  $\text{SiCl}_4$  input rate is larger than  $0.42 \text{ mol h}^{-1}$ . The deposition rate is much higher than that of APTPECVD with  $\text{CH}_4$  as the carbon source at the same  $\text{SiCl}_4$  input rate, which may be caused by the formation of more porous film structures with  $\text{C}_2\text{H}_2$  as the carbon source.

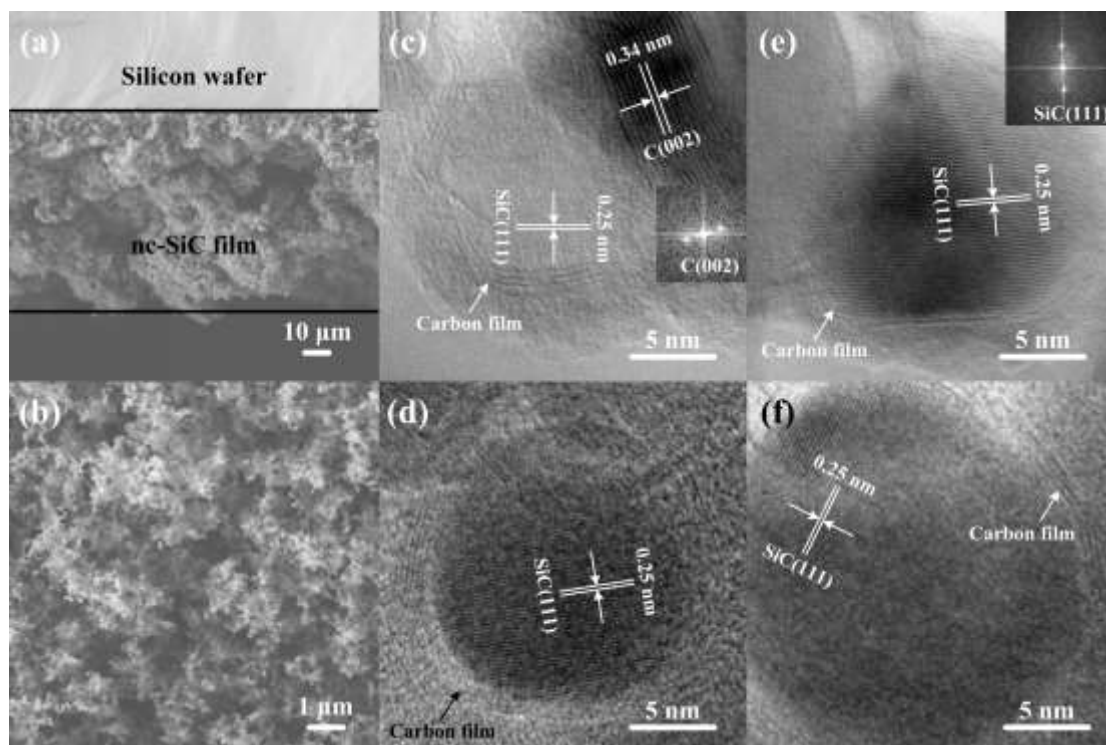


Fig. 2 (a) Typical cross-sectional SEM image of the sample at  $\text{SiCl}_4$  input rate of  $0.52 \text{ mol h}^{-1}$ ; (b) SEM image of sample at  $\text{SiCl}_4$  input rate of  $0.31 \text{ mol h}^{-1}$ ; typical bright-field TEM images with associated FFT patterns of samples at  $\text{SiCl}_4$  input rates of (c)  $0.10 \text{ mol h}^{-1}$ , (d)  $0.21 \text{ mol h}^{-1}$ , (e)  $0.31 \text{ mol h}^{-1}$  and (f)  $0.42 \text{ mol h}^{-1}$ .

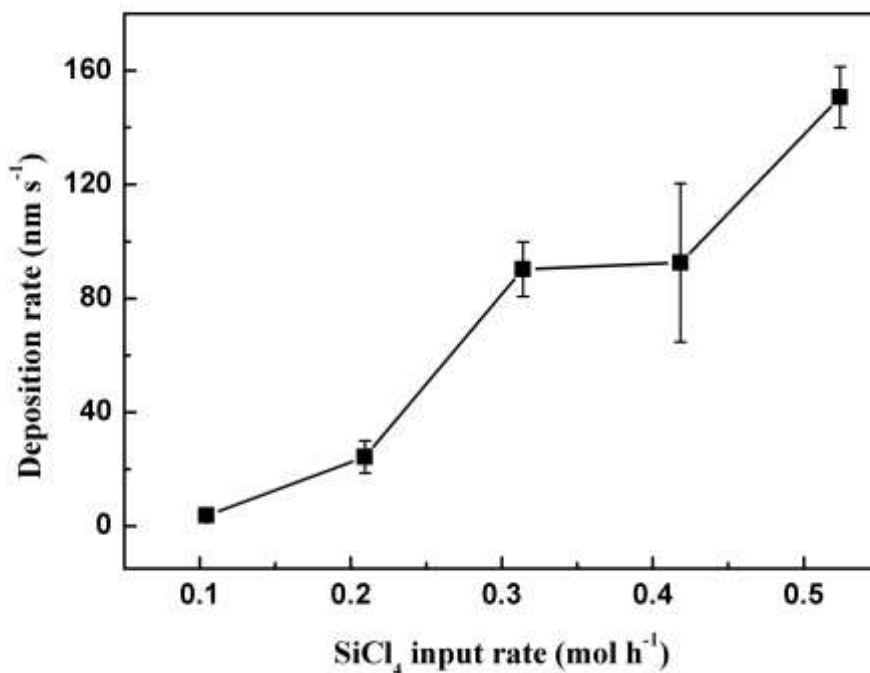


Fig. 3 Effect of SiCl<sub>4</sub> input rate on deposition rate of thin film complex.

X-ray photoelectron spectroscopy (XPS) was applied to analyze the surface chemical composition of the samples and the results are given in Fig. 4. Si, C and O are found on the surface and their chemical states can be studied by deconvolution of the spectra. Si 2p spectrum is fitted into peaks at 100.79 eV, 102.69 eV and 103.68 eV corresponding to Si-C in SiC, Si-O in SiO<sub>x</sub> and Si-O in SiO<sub>2</sub>, respectively.<sup>44-46</sup> Si-O is formed through the oxidation of surface dangling bonds during the samples' contact with air.<sup>37</sup> This explains the occurrence of O on the surface. As can be seen from the O 1s spectrum in Fig. 4 (d), O atom mainly exists in Si-O of SiO<sub>2</sub>. No peak of Si-Si is observed in Si 2p spectrum, which means that no a-Si exists on the sample's surface. XPS is known to be a surface-sensitive technique that analyzes only the top 0-10 nm of the sample. The surface of the samples is oxidized in air, which may result in the fact that surface Si only appears in the form of SiC and SiO<sub>x</sub>. C 1s spectrum is fitted into peaks at 283.79 eV, 284.93 eV and 286.17 eV

corresponding to Si-C in SiC, C-C in graphite and C-H.<sup>47, 48</sup> As can be seen from Fig. 4 (c), the peak of C-C in graphite has the largest area, which means that C mainly exists in the form of graphite in the thin film complex. XPS analysis results agree well with XRD and TEM characterization results. Moreover, the surface mole fractions of C and SiC could be calculated. The surface C mole fraction is defined as the relative mole fraction of C on the surface divided by the total mole concentration of surface C and Si while the surface SiC mole fraction is defined as the relative mole concentration of Si in Si-C of SiC divided by the combined mole concentration of Si-O in SiO<sub>x</sub> and SiO<sub>2</sub>. The effect of SiCl<sub>4</sub> input rate on surface mole fractions of C and SiC is shown in Fig. 5. The surface C mole fraction first increases then decreases with increasing SiCl<sub>4</sub> input rate. This indicates that the increase of SiCl<sub>4</sub> input rate would intensify the decomposition of C<sub>2</sub>H<sub>2</sub> at first stage. However, more Si is deposited while SiCl<sub>4</sub> keeps increasing which results in the increase of Si mole fraction in the sample and the decrease of C mole fraction. The surface SiC mole fraction increases with increasing SiCl<sub>4</sub> input rate and reaches a maximum at SiCl<sub>4</sub> input rate of 0.42 mol h<sup>-1</sup>, then the mole fraction decreases when SiCl<sub>4</sub> input rate keeps increasing. This result explains the effect of SiCl<sub>4</sub> input rate on XRD peaks intensities of β-SiC. A larger amount of Si will be produced in the gas phase at higher SiCl<sub>4</sub> input rate so that more SiC will be formed. However, the carbon amount may be insufficient as too much Si exists in the gas phase, which will lead to the formation of a-Si other than SiC and cause the decrease of SiC mole fraction.

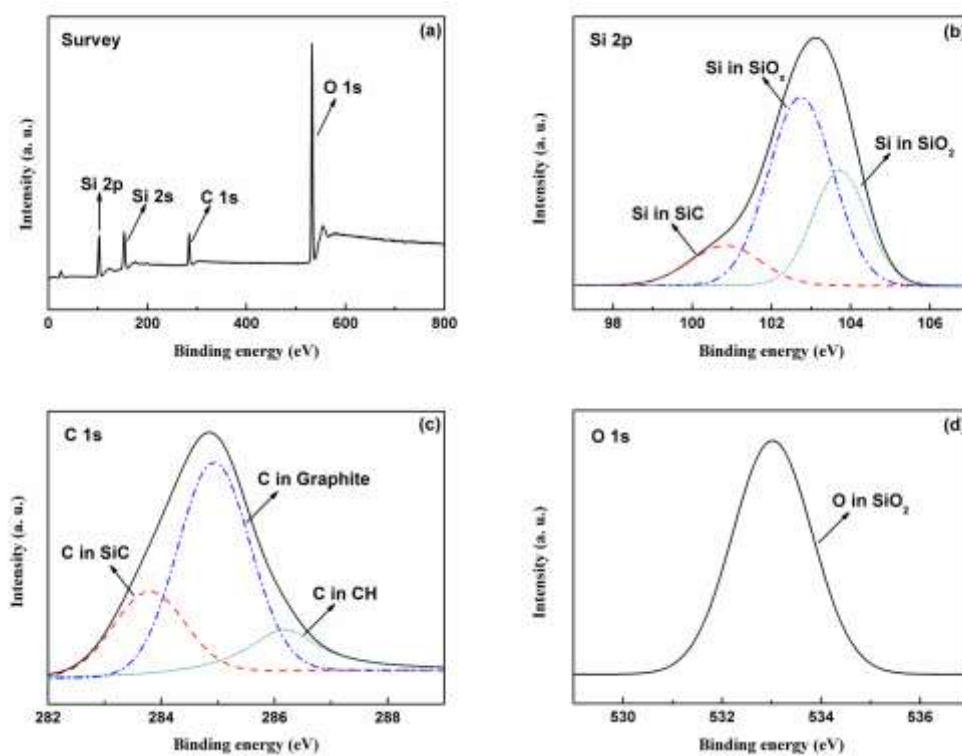


Fig. 4 (a) Survey XPS spectrum of sample at  $\text{SiCl}_4$  input rate of  $0.42 \text{ mol h}^{-1}$  and spectra of (b) Si 2p, (c) C 1s and (d) O 1s.

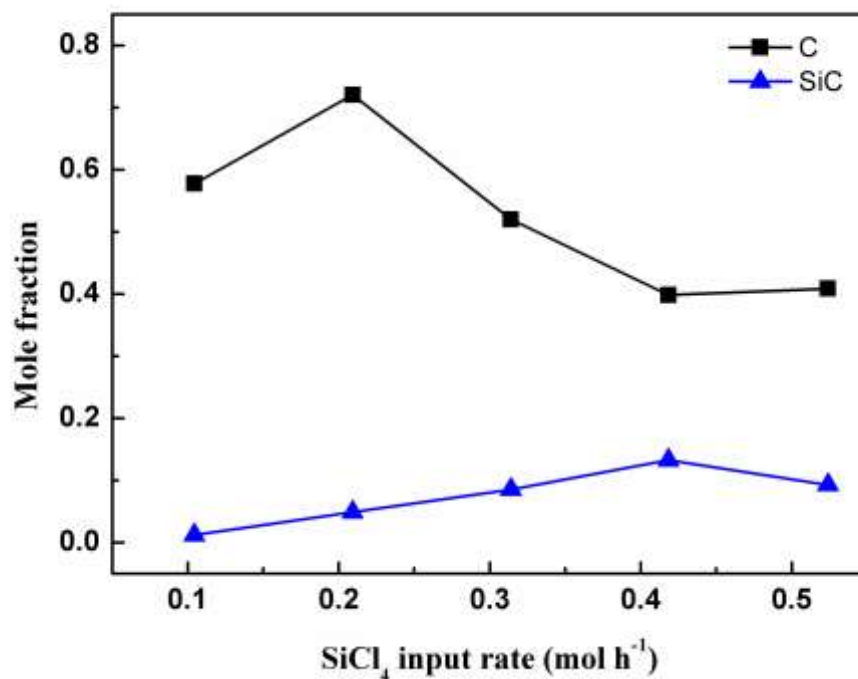


Fig. 5 Effect of SiCl<sub>4</sub> input rate on (a) surface C atomic fraction and (b) surface SiC mole fraction of samples.

The PL property of SiC nanocrystals suspended in ethanol was further studied. The excitation is in the ultra-violet (UV) wavelength region and the effect of excitation wavelength was studied. As shown in Fig. 6, the emission shows a small red shift as the excitation moves toward 280 nm, which agrees well with the prediction of quantum confinement effect<sup>17</sup>. A strong PL in red wavelength region with the excitation of 280 nm laser is observed, as shown in Fig. 6. This red region emission originates from quantum confinement effects of SiC nanocrystals in the sample. The relatively larger average diameter makes the samples' PL in red region, which differs from SiC quantum dots' UV-green region emission.<sup>17, 22</sup> Red region emission is desirable for *in vivo* studies since photons in this region can penetrate deeply in organic tissues.<sup>25</sup> This shows the potential application of APTPECVD SiC nanocrystals in bioimaging and drug delivery.

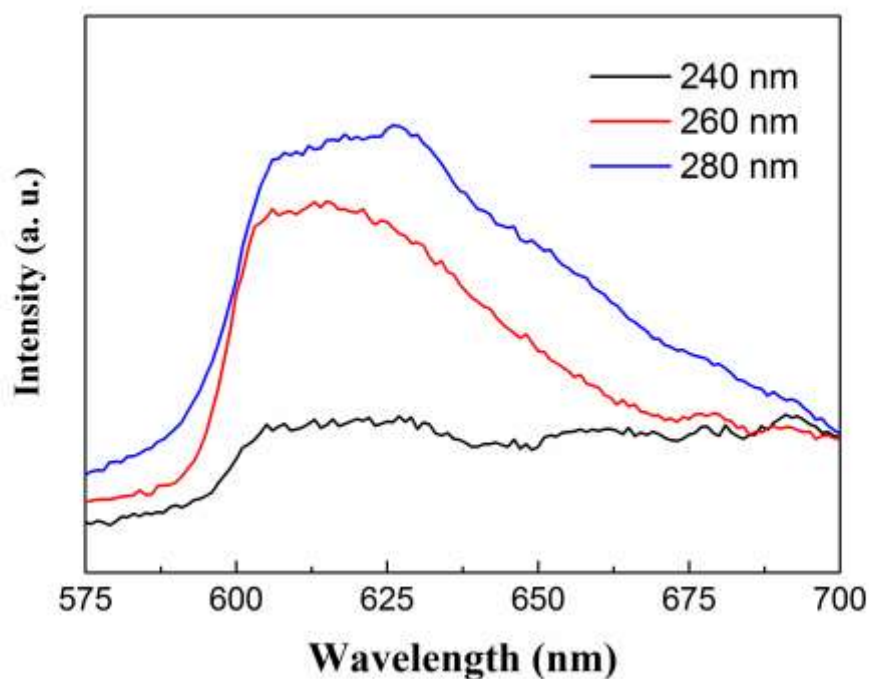


Fig. 6 PL spectra of SiC nanocrystals deposited at  $\text{SiCl}_4$  input rate of  $0.31 \text{ mol h}^{-1}$  and suspended in ethanol with different excitation wavelength.

When applied in *in vivo* system, the thin film complex should be purified to obtain pure SiC nanocrystals. Fig. 7 shows the thermal gravity analysis (TGA) results of samples at different  $\text{SiCl}_4$  input rates. The largest weight-loss ratio is observed in the temperature range of  $550\text{-}650 \text{ }^\circ\text{C}$ , which is the main decomposition temperature of C in oxygen. Since both C and a-Si could be oxidized, a post-treatment including calcination and HF solution etching was carried out to remove C and a-Si from the complex. The sample was first calcined in air at  $650 \text{ }^\circ\text{C}$  to oxidize a-Si to  $\text{SiO}_2$  and to remove C. Then, the calcined sample was treated by 20% HF solution to remove  $\text{SiO}_2$ . Finally, pure SiC nanocrystals were obtained after washing and drying.

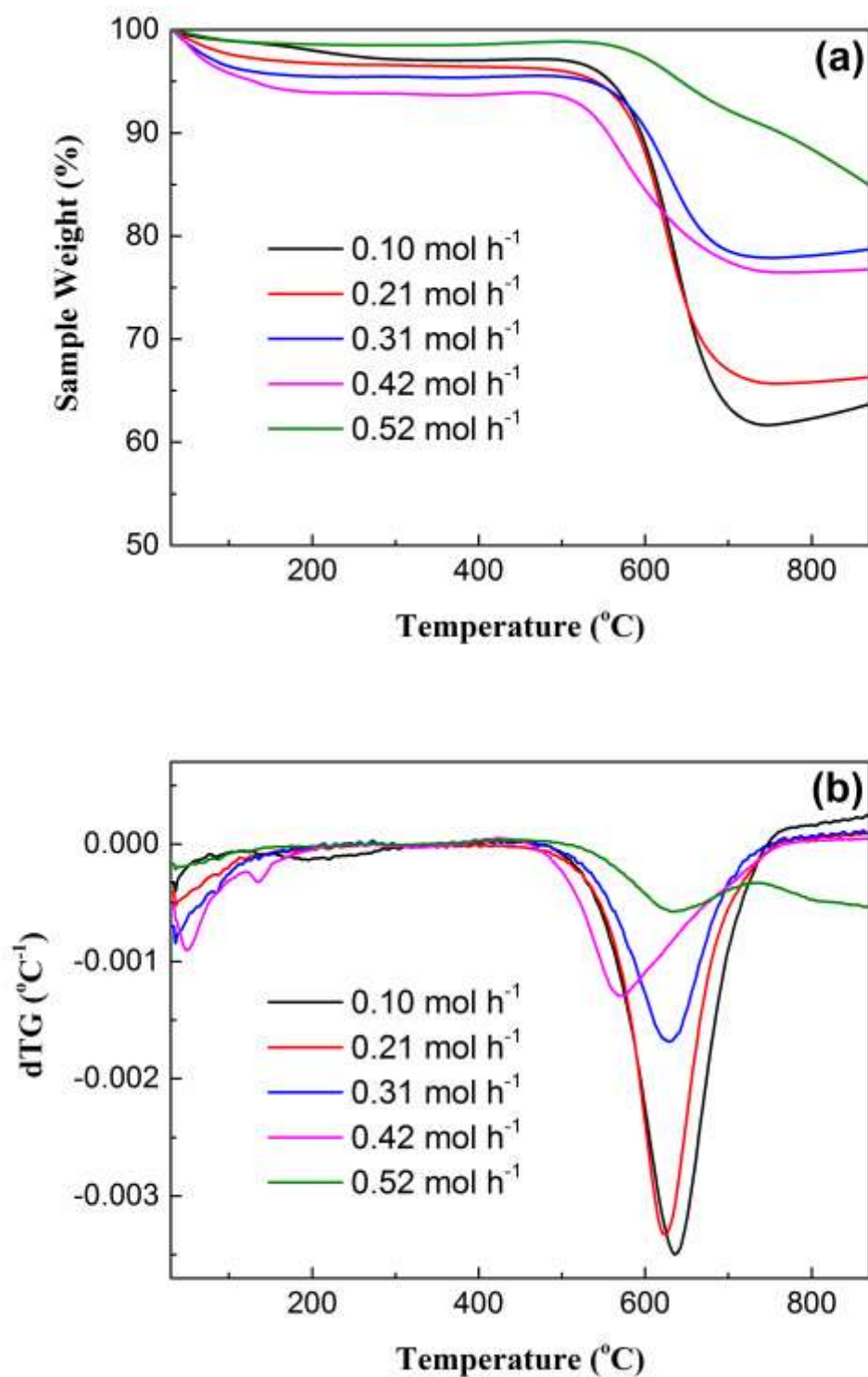


Fig. 7 (a) TGA spectra in  $\text{O}_2$  atmosphere and (b) the 1<sup>st</sup> derivative curve of TGA spectra of samples at different  $\text{SiCl}_4$  input rates.

TEM images of samples before and after post-treatment are given in Fig. 8. Before post-treatment, SiC nanocrystals are covered by carbon films and embedded in a complex consisting of a-Si and graphite. After post-treatment, carbon films covering SiC nanocrystals disappear and so does the skeleton complex consisting of a-Si and graphite. Thus, pure SiC nanocrystals can be fabricated combining APTPECVD and a simple post-treatment process. Clear lattice fringes of  $\beta$ -SiC (111) crystal plane are observed. Meanwhile, FFT results show clear diffraction pattern of  $\beta$ -SiC (111) crystal plane. PL property of samples after post-treatment is shown in Fig. 9. The samples after treatment still have emission in red region while the emission shows a small blue-shift compared with raw samples. The high temperature calcination process may affect the crystal structure and defect state of SiC nanocrystals resulting in the change of PL property.

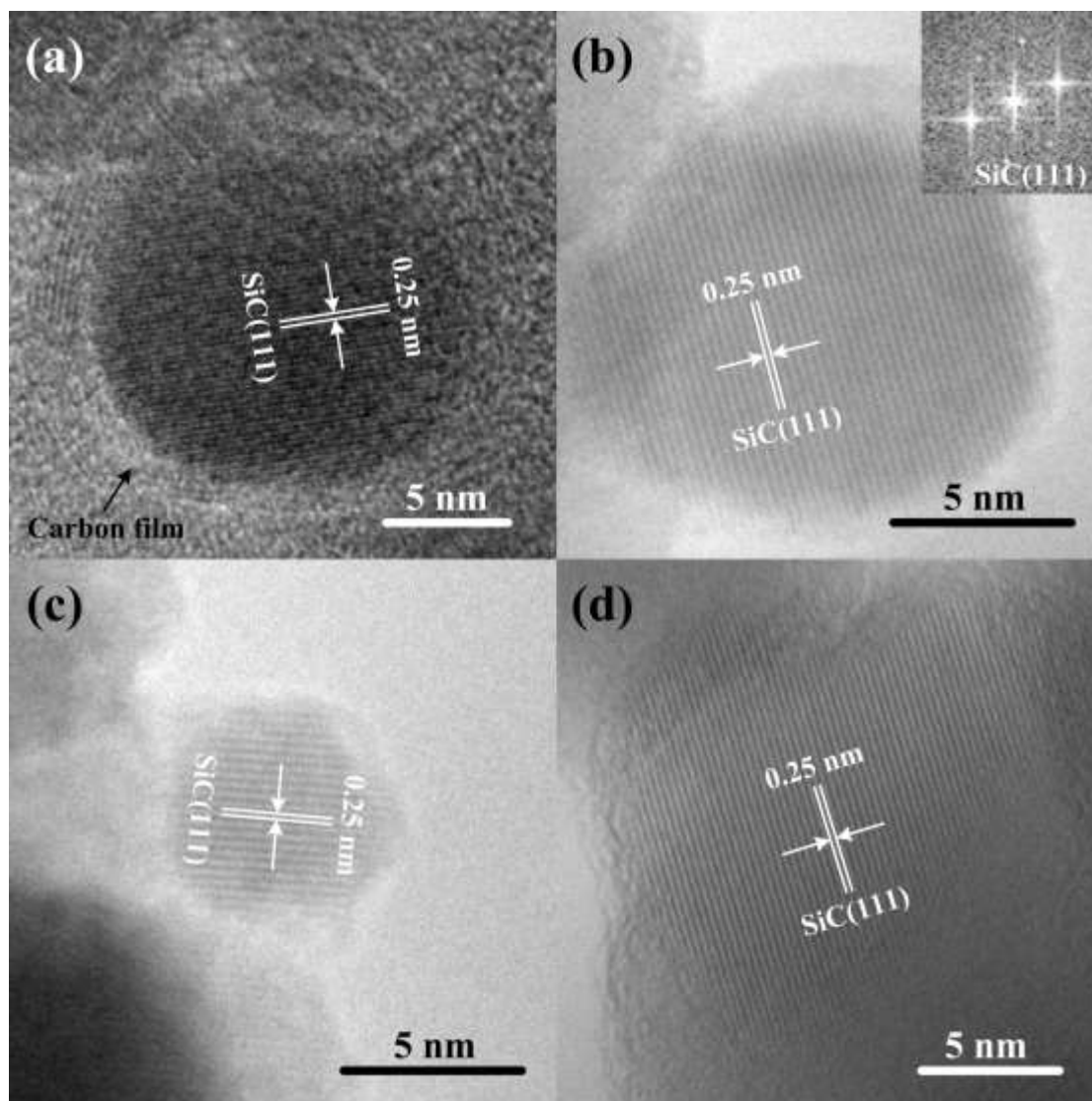


Fig. 8 Bright-field TEM images with associated FFT patterns of (a) raw samples at SiCl<sub>4</sub> input rates of 0.31 mol h<sup>-1</sup>, (b)(c)(d) samples at SiCl<sub>4</sub> input rates of 0.21, 0.31 and 0.42 mol h<sup>-1</sup> after post-treatment.

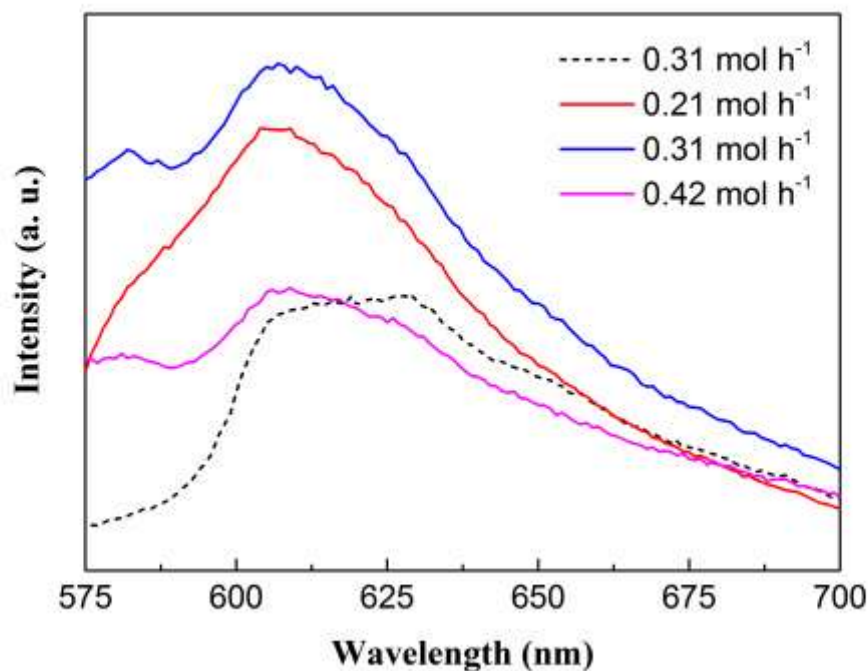


Fig. 9 PL spectra of samples before (dash line) and after (solid lines) post-treatment at different SiCl<sub>4</sub> input rates.

## Experimental

### Fabrication of SiC nanocrystals

SiC nanocrystals were fabricated by APTPECVD with thermal plasma generated by 10 kW RF plasma source. Detailed information of this APTPECVD apparatus could be found elsewhere.<sup>36</sup> The plasma working gas was Ar. SiCl<sub>4</sub> and C<sub>2</sub>H<sub>2</sub> diluted by H<sub>2</sub> were used as silicon source and carbon source, respectively. SiCl<sub>4</sub> input rate was changed from 0.10 to 0.52 mol h<sup>-1</sup> to study its effect on deposition process. The input rates of C<sub>2</sub>H<sub>2</sub> and H<sub>2</sub> were fixed at 0.13 mol h<sup>-1</sup> and 2.27 mol h<sup>-1</sup>. Both (111) c-Si and glass were used as substrates.

### Post-treatment

The post-treatment includes both calcination and etching processes. First, the sample was calcined at 650 °C for 3 h in air, during which C was oxidized to CO<sub>2</sub>/CO and a-Si was oxidized to SiO<sub>2</sub>. Then, the sample was etched by 20% HF solution at room temperature with ultrasonic vibration for 30 min to remove SiO<sub>2</sub>. The ultrasonic frequency was 80 kHz. The solution with suspended nanocrystals was centrifuged at 8,000 rpm for 5 min to remove surplus acid. The obtained nanocrystals were washed and dried at 70 °C for hours. Finally, ethanol was added to suspend the SiC nanocrystals with ultrasonic vibration for 30 min.

### Characterization

The microstructure of the samples were characterized by SEM (JSM-6460LV) and TEM (JEM-2010). The crystal structure of the samples were analyzed by XRD (Bruker D8 Advance) with monochromatized Cu K $\alpha$  radiation and Raman spectroscopy (Horibra LABRAM-HR) with 532 nm He-Ne laser excitation. The surface chemistry of the samples was analyzed using XPS (ESCALAB 250Xi) with Al K $\alpha$  radiation, and the C 1s peak at 284.6 eV was used as an internal standard.

### Conclusion

SiC nanocrystals have superior chemical, physical and mechanical properties, *e.g.* biocompatibility and PL property, which have various potential applications in electronic and biological systems. In this work, thin film complex consisting SiC nanocrystals, a-Si and graphite was fabricated by APTPECVD with deposition rates up to 150 nm s<sup>-1</sup>. The SiC nanocrystals have average diameters in the range of 18-30 nm. The effect of SiCl<sub>4</sub> input rate on deposition rate and product properties was studied. A room temperature red region PL property of SiC nanocrystals was observed with 280 nm laser excitation. After a simple post-treatment process, C and a-Si were

removed from the complex and pure SiC nanocrystals were obtained. These SiC nanocrystals fabricated by APTPECVD with red region emission have potential applications in *in vivo* systems such as biomarkers for bioimaging and drug delivery.

## Acknowledgements

This study was supported by the National Basic Research Program of China (973 Program no. 2012CB720301), the National Natural Science Foundation of China (NSFC) under grant no. 21176137. We are also grateful for Mr Zezhong Cao's help on the deposition experiments.

## References:

1. D. Nakamura, I. Gunjishima, S. Yamaguchi, T. Ito, A. Okamoto, H. Kondo, S. Onda and K. Takatori, *Nature*, 2004, **430**, 1009-1012.
2. R. Madar, *Nature*, 2004, **430**, 974-975.
3. S. Castelletto, B. C. Johnson, V. Ivady, N. Stavrias, T. Umeda, A. Gali and T. Ohshima, *Nat. Mater.*, 2014, **13**, 151-156.
4. F. Fuchs, V. A. Soltamov, S. Vaeth, P. G. Baranov, E. N. Mokhov, G. V. Astakhov and V. Dyakonov, *Sci. Rep.-UK*, 2013, **3**, 1637.
5. C. R. Eddy and D. K. Gaskill, *Science*, 2009, **324**, 1398-1400.
6. H. W. Shim, K. C. Kim, Y. H. Seo, K. S. Nahm, E. K. Suh and H. J. Lee, *Appl. Phys. Lett.*, 1997, **70**, 1757-1759.
7. A. L. Falk, B. B. Buckley, G. Calusine, W. F. Koehl, V. V. Dobrovitski, A. Politi, C. A. Zorman, P. X. L. Feng and D. D. Awschalom, *Nat. Commun.*, 2013, **4**, 1819.
8. P. G. Baranov, A. P. Bundakova, A. A. Soltamova, S. B. Orlinskii, I. V. Borovykh, R. Zondervan, R. Verberk and J. Schmidt, *Phys. Rev. B*, 2011, **83**, 125203.
9. T. Matsumoto, J. Takahashi, T. Tamaki, T. Futagi, H. Mimura and Y. Kanemitsu, *Appl. Phys. Lett.*, 1994, **64**, 226-228.
10. Y. P. Guo, J. C. Zheng, A. Wee, C. Huan, K. Li, J. S. Pan, Z. C. Feng and S. J. Chua, *Chem. Phys. Lett.*, 2001, **339**, 319-322.
11. J. Zhu, Z. Liu, X. L. Wu, L. L. Xu, W. C. Zhang and P. K. Chu, *Nanotechnology*, 2007, **18**, 365603.
12. D. J. Dai, N. Zhang, W. X. Zhang and J. Y. Fan, *Nanoscale*, 2012, **4**, 3044-3046.
13. J. Zhu, S. Hu, W. Xia, T. Li, L. Fan and H. Chen, *Mater. Lett.*, 2014, **132**, 210-213.
14. X. Guo, D. Dai, B. Fan and J. Fan, *Appl. Phys. Lett.*, 2014, **105**, 193110.
15. S. Castelletto, Z. Bodrog, A. P. Magyar, A. Gentle, A. Gali and I. Aharonovich, *Nanoscale*, 2014, **6**, 10027-10032.
16. S. Castelletto, B. C. Johnson, C. Zachreson, D. Beke, I. Balogh, T. Ohshima, I. Aharonovich and A. Gali, *ACS Nano.*, 2014, **8**, 7938-7947.

17. X. L. Wu, J. Y. Fan, T. Qiu, X. Yang, G. G. Siu and P. K. Chu, *Phys. Rev. Lett.*, 2005, **94**, 0261022.
18. J. S. Shor, L. Bemis, A. D. Kurtz, I. Grimberg, B. Z. Weiss, M. F. Macmillian and W. J. Choyke, *J. Appl. Phys.*, 1994, **76**, 4045-4049.
19. A. O. Konstantinov, C. I. Harris and E. Janzen, *Appl. Phys. Lett.*, 1994, **65**, 2699-2701.
20. D. H. Feng, Z. Z. Xu, T. Q. Jia, X. X. Li and S. Q. Gong, *Phys. Rev. B*, 2003, **68**, 0353343.
21. X. L. Wu, Y. Gu, S. J. Xiong, J. M. Zhu, G. S. Huang, X. M. Bao and G. G. Siu, *J. Appl. Phys.*, 2003, **94**, 5247.
22. J. Y. Fan, H. X. Li, J. Iiang, L. So, Y. W. Lam and P. K. Chu, *Small*, 2008, **4**, 1058-1062.
23. J. Y. Fan and P. K. Chu, *Small*, 2010, **6**, 2080-2098.
24. B. Somogyi, V. Zolyomi and A. Gali, *Nanoscale*, 2012, **4**, 7720-7726.
25. D. Beke, Z. Szekrenyes, D. Palfi, G. Rona, I. Balogh, P. A. Maak, G. Katona, Z. Czigany, K. Kamaras, B. Rozsa, L. Buday, B. Vertessy and A. Gali, *J. Mater. Res.*, 2013, **28**, 205-209.
26. B. Mognetti, A. Barberis, S. Marino, F. Di Carlo, V. Lysenko, O. Marty and A. Geloan, *J. Nanosci. Nanotechnol.*, 2010, **10**, 7971-7975.
27. T. Serdiuk, V. Lysenko, B. Mognetti, V. Skryshevsky and A. Geloan, *J. Biophotonics*, 2013, **6**, 291-297.
28. S. Xu, K. Ostrikov, J. D. Long and S. Y. Huang, *Vacuum*, 2006, **80**, 621-630.
29. Q. Cheng, S. Xu, J. Long and K. K. Ostrikov, *Appl. Phys. Lett.*, 2007, **90**, 173112.
30. T. Takeshita, K. Ichige, Y. Kurata and S. Hasegawa, *J. Appl. Phys.*, 1991, **69**, 7945-7947.
31. K. L. Cheng, H. C. Cheng, W. H. Lee, C. P. Lee, C. C. Liu and T. R. Yew, *Appl. Phys. Lett.*, 1997, **70**, 223-225.
32. S. Kerdiles, A. Berthelot, F. Gourbilleau and R. Rizk, *Appl. Phys. Lett.*, 2000, **76**, 2373-2375.
33. T. Rajagopalan, X. Wang, B. Lahlouh, C. Ramkumar, P. Dutta and S. Gangopadhyay, *J. Appl. Phys.*, 2003, **94**, 5252-5260.
34. K. Ostrikov, J. D. Long, P. P. Rutkevych and S. Xu, *Vacuum*, 2006, **80**, 1126-1131.
35. M. Shigeta and A. B. Murphy, *J. Phys. D Appl. Phys.*, 2011, **44**, 17400117.
36. T. Cao, H. Zhang, B. Yan and Y. Cheng, *RSC Adv.*, 2013, **3**, 20157-20162.
37. T. Cao, H. Zhang, B. Yan, W. Lu and Y. Cheng, *RSC Adv.*, 2014, **4**, 49228-49235.
38. T. Cao, H. Zhang, B. Yan, W. Lu and Y. Cheng, *RSC Adv.*, 2014, **4**, 15131-15137.
39. H. Fritzsche, M. Tanielian, C. C. Tsai and P. J. Gaczi, *J. Appl. Phys.*, 1979, **50**, 3366-3369.
40. E. Bustarret, M. A. Hachicha and M. Brunel, *Appl. Phys. Lett.*, 1988, **52**, 1675-1677.
41. A. C. Ferrari, J. C. Meyer, V. Scardaci, C. Casiraghi, M. Lazzeri, F. Mauri, S. Piscanec, D. Jiang, K. S. Novoselov, S. Roth and A. K. Geim, *Phys. Rev. Lett.*, 2006, **97**, 18740118.
42. A. C. Ferrari and J. Robertson, *Phys. Rev. B*, 2000, **61**, 14095-14107.
43. S. Nakashima and H. Harima, *Phys. Status Solidi A*, 1997, **162**, 39-64.
44. Z. H. Wen, G. H. Lu, S. M. Cui, H. Kim, S. Q. Ci, J. W. Jiang, P. T. Hurley and J. H. Chen, *Nanoscale*, 2014, **6**, 342-351.
45. A. A. Galuska, J. C. Uht and N. Marquez, *J. Vac. Sci. Technol. A*, 1988, **6**, 110-122.
46. X. R. Yu and H. Hantsche, *Surf. Interface Anal.*, 1993, **20**, 555-558.
47. L. Muehlhoff, W. J. Choyke, M. J. Bozack and J. T. Yates, *J. Appl. Phys.*, 1986, **60**, 2842-2853.
48. J. A. Taylor, G. M. Lancaster and J. W. Rabalais, *Appl. Surf. Sci.*, 1978, **1**, 503-514.